THE JOURNAL OF PHYSICAL CHEMISTRY B

Article

pubs.acs.org/JPCB

HIV-TAT Enhances the Transdermal Delivery of NSAID Drugs from Liquid Crystalline Mesophases

Marganit Cohen-Avrahami,[†] Alexander I. Shames,[‡] M. Francesca Ottaviani,[§] Abraham Aserin,[†] and Nissim Garti*[,†]

[†]Casali Institute of Applied Chemistry, The Institute of Chemistry, The Hebrew University of Jerusalem, Edmond J. Safra Campus, Givat Ram, Jerusalem 9190401, Israel

[‡]Department of Physics, Ben-Gurion University of the Negev, P.O. Box 653, Beer-Sheva 84105, Israel

[§]Department of Earth, Life and Environment Sciences, University of Urbino, Località Crocicchia, Urbino 61029, Italy

Supporting Information

ABSTRACT: Sodium diclofenac (Na-DFC) and celecoxib (CLXB) are common nonsteroidal anti-inflammatory (NSAID) drugs which suffer from poor bioavailability and severe side effects when consumed orally, and their transdermal delivery might present important advantages. In this study, the drugs were solubilized in cubic and lamellar mesophases as transdermal delivery vehicles, and a cell-penetrating peptide, HIV-TAT (TAT), was examined as a skin penetration enhancer. SD-NMR, ATR-FTIR, and EPR measurements revealed that, in the cubic mesophase (which is rich in water content), TAT populates the aqueous cores and binds water, while in the dense lamellar system (with the lower water content) TAT is bound also to the glycerol monooleate (GMO) and increases the microviscosity and the order degree. TAT secondary structure in the cubic system was found to be a random coil while once it was embedded in the closely packed lamellar system it transforms to a more ordered compact state of β-turns arranged around the GMO headgroups. TAT remarkably increased the diffusion of Na-DFC and CLXB from the cubic systems by 6- and 9-fold enhancement, respectively. TAT effect on drug diffusion from the lamellar systems was limited to an increase of 1.3- and 1.7-fold, respectively. The dense packing and strong binding in the lamellar phase led to slow diffusion rates and slower drug release in controlled pattern. These effects of the chemical composition and vehicle geometry on drug diffusion are demonstrated with the impacts of TAT which can be specifically utilized for controlling skin delivery of drugs as required.

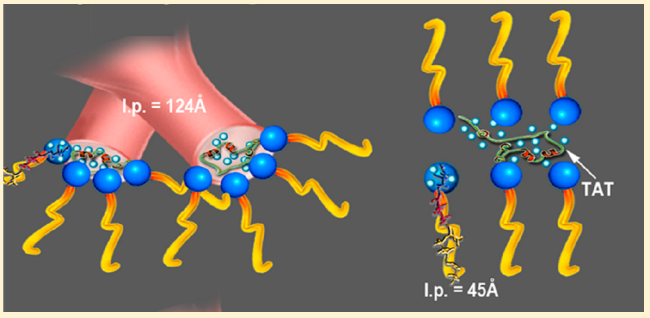

1. INTRODUCTION

The glycerol monooleate (GMO)-based lyotropic liquid crystals are promising gels comprising an extremely large surface area which can be utilized for developing transdermal delivery vehicles.[1−3] The advantages of transdermal delivery are wide along with the safe and low-cost GMO lipid, which provides an appropriate matrix for drug solubilization.[4−6] GMO easily swells with the addition of water and forms several nanostructured systems depending on water content and on temperatures. Yet, the binary systems exhibit many strong hydrogen bonds and are very stiff, rigid gels, thus complicating their practical applicability. The addition of ethanol to the mesophases enables the formation of soft gels, with cubic or lamellar symmetry, which can comfortably be rubbed on the skin. Many researchers utilized the GMO-based mesophases for the solubilization of bioactives and demonstrated the potential of these systems for transdermal delivery of a variety of drugs.[7−11]

This research focuses on two nonsteroidal anti-inflammatory (NSAID) drugs, sodium diclofenac (Na-DFC) and celecoxib (CLXB), which are very potent and widely used medications, mainly for reducing pain and inflammation, yet their low solubility in water decreases their effectiveness and forces the orally consumed dose to be unfavorably high.[12−14] Their oral intake is associated with some severe side effects such as ulcers and gastrointestinal bleeding,[15,16] and the transdermal delivery, bypassing the first-pass metabolism along with lower dosage, might be highly advantageous, decreasing the side effects and increasing patient compliance.[17,18]

The purpose is to deliver a sufficient amount of the drug (within the lipid vehicle, which has a high loading capacity and is easily rubbed on the skin) to the stratum corneum (the outer skin layer). The drug should accumulate in the stratum corneum and diffuse into the tissue, for providing topical therapeutic activity; TAT peptide is designated as the skin

Received: December 29, 2013
Revised: May 4, 2014
Published: May 5, 2014

   dx.doi.org/10.1021/jp412739p | J. Phys. Chem. B 2014, 118, 6277−6287

permeating agent for enabling higher loads in the stratum corneum and increased skin permeation of the drug.

The solubilization of Na-DFC and CLXB within the cubic and the lamellar systems was previously investigated and characterized.[19] The tendency of CLXB to diffuse out of the mesophases toward the skin was much lower than Na-DFC diffusion. Interestingly, the cubic mesophase revealed increased diffusion of Na-DFC, compared to the dense lamellar phase. The suggestion was that, whereas Na-DFC diffuses through the aqueous channels and is strongly affected by the diffusion coefficient of the water, CLXB diffuses through the lipid lipophilic domains and its diffusion was not affected by the system hydration, and any effort to increase its diffusivity should focus on the lipophilic mesophase regions.

In order to further increase the skin permeation of Na-DFC and CLXB, TAT peptide was chosen. TAT is a prominent member of the family of cell penetrating peptides (CPPs).[20−22] This special type of peptide, first discovered in biological systems as HIV, has the ability to penetrate cell membranes.[23,24] TAT is the trans-activating transcriptional activator protein from HIV-1, and its sequence is GRKKRRQRRRPPQ (residues 48−60).[25] This "arginine-rich" sequence is essential for virus replication due to its role in the transactivation of DNA transcription[26] and is directly involved in protein−protein recognition processes[27] and RNA binding *in vivo*.[28,29] The low-toxicity TAT is very effective in penetrating cell membranes and inserting various molecules into living cells and cell nuclei in a noncovalent manner.[30−32] The high concentration of arginine, or any basic positively charged amino acids, is a typical feature of the cell penetrating peptides and probably plays a role in the initial attachment of the peptide to the negatively charged cell membrane.[33−36] The ability of several CPPs to enhance delivery through skin was already examined and proved, and different mechanisms were suggested. These features make the CPP family very attractive in the field of transdermal delivery. TAT was already utilized in attachment to nanoparticles for enhancing their delivery through skin.[37,38]

This study examines the ability of TAT to increase the transdermal delivery of drugs when it is not covalently linked to them, but is solubilized together with the drug within the transdermal carrier. The liquid crystalline mesophases serve as the hosting gel carriers which can easily be applied on the skin, and TAT, loaded within the carrier, is examined as a skin penetration enhancer for Na-DFC and CLXB from the mesophases. The structural effects which TAT induces on the mesophases, in addition to the TAT secondary structures within the hosting gels, were explored. The permeability of Na-DFC and CLXB through porcine skin was determined *in vitro* using Franz diffusion cells.

2. MATERIALS AND METHODS

GMO (distilled glycerol monooleate) consisting of 97.1 wt % monoglycerides, 2.5 wt % diglycerides, and 0.4 wt % free glycerol (acid value 1.2, iodine value 68.0, melting point 37 °C) was obtained from Riken Vitamin Co. Ltd. (Tokyo, Japan). (The free fatty acid content was shown not to increase once water was embedded in the core of the mesophases because the water is mostly bound with low activity.) Ethanol (EtOH; analytical reagent >99%) was purchased from Frutarom Ltd. (Haifa, Israel). Na-DFC was purchased from Sigma (St. Louis, MO, USA). CLXB was a kind gift from Trima Israel Pharmaceutical Products (Kibbutz Maabarot, Israel). TAT peptide (>95% purity) was synthesized by GL Biochem (Shanghai, China). D_2O (D, 99.9%) was purchased from Cambridge Isotope Laboratories, Inc. (Andover, MA, USA). The spin probe 5-doxylstearic acid [2-(3-carboxypropyl)-4,4-dimethyl-2-tridecyl-3-oxazolidinyloxy], free radical, was purchased from Sigma-Aldrich (St. Louis, MO, USA). Phosphate buffered saline (PBS) was purchased from Biological Industries (Kibbutz Beit Haemek, Israel). High-performance liquid chromatography (HPLC) grade solvents (water and acetonitrile) were obtained from J.T. Baker (Mallinckrodt Baker, Inc., Phillipsburg, NJ, USA) and Merck (Darmstadt, Germany). Trifluoroacetic acid (TFA) was purchased from Fluka (Buchs, Switzerland). The water was double distilled. All chemicals were used without further purification. Porcine skins were purchased from Lahav Research Institute (Kibbutz Lahav, Israel). The skin was excised from ears of domestic white pigs, carefully dissected and dermatomized, stored at −20 °C, and used within a month.

2.1. Preparation of the Mesophases. The chosen compositions for preparing the lyotropic liquid crystals mesophases were based on GMO, EtOH, and water at concentration ratios of 57:5:38 wt %, respectively, for the cubic mesophase, and 70:10:20 for the lamellar mesophase. These compositions were chosen as they are stable, soft gels which can be comfortably rubbed on the skin, and they exhibit high loading capacities for the NSAID drugs (Na-DFC and CLXB) and for the TAT peptide. The mesophases were prepared by mixing weighed quantities of the components, preheated to 45 °C, in sealed tubes under nitrogen atmosphere to avoid oxidation of the GMO. Na-DFC and CLXB were dissolved in the GMO before mixing. TAT was dissolved in the water before mixing. It should be noted that, as a result of Na-DFC, CLXB, and TAT solubilization, the concentrations of GMO, ethanol, and water were decreased, yet their weight ratio was kept constant. The different structures were confirmed by SAXS, 24 h after preparation.

2.2. SAXS. SAXS experiments were performed using a Be-filtered Cu Kα radiation (0.154 nm) from a rotating anode X-ray generator that operated at a power rating of 1.2 kW. The rotating anode diameter was 99 mm, and its rotation speed was 9000 rpm. The electron gun was a W filament. The X-ray radiation was further monochromated and collimated by Confocal Max-Flux Optics from Rigaku Inc. (Tokyo, Japan) and measured by a Mar345 Image Plate Detector from Marresearch (Norderstedt, Germany). The samples were held in 1.5 mm quartz X-ray capillaries inserted into an aluminum block sample holder. The camera constants were calibrated using silver behenate. The scattering patterns were processed in the fit2d software.

2.3. SD-NMR. The diffusion coefficients of the different mesophase components were determined within the cubic and the lamellar mesophases at increasing TAT concentrations. All SD-NMR experiments were performed with a Bruker Avance II spectrometer equipped with GREAT 1/10 gradients (Frankfurt, Germany) at a spinning rate of 4000 Hz with a 4 mm HR-MAS probe with a shielded magic-angle gradient with a maximum strength of 0.639 T m^{-1}. Diffusion was measured in an asymmetric bipolar LED experiment with an asymmetry factor of 20%, ramping the strongest gradient from 2% to 95% of the maximum strength in 32 steps. The spectrum was processed by a Fourier transform in the acquisition (t_2) dimension and by a Levenberg−Marquardt fit to decaying Gaussians with the Bruker TOPSPIN software, in the gradient

dx.doi.org/10.1021/jp412739p | J. Phys. Chem. B 2014, 118, 6277−6287

ramp evolution (g) dimension. NMR spectra were recorded within the range of 25−65 °C. At the SD-NMR measurements, the water was replaced with D_2O. All self-diffusion coefficients reported here are reproducible with an error range of ±2.5%.

2.4. Attenuated Total Reflectance Fourier Transform Infrared (ATR-FTIR) Measurements. An Alpha P model infrared spectrophotometer, equipped with a single reflection diamond ATR sampling module, manufactured by BrukerOptik GmbH (Ettlingen, Germany), was used to record the FTIR spectra. The spectra were recorded with 50 scans at 25 °C; a spectral resolution of ±2 cm^{-1} was obtained. Multi-Gaussian fitting has been utilized to resolve individual bands in the spectra. The peaks were analyzed in terms of peak frequencies, width at half-height, and area.

TAT secondary structures were determined using the amide I band as the samples' spectra were background subtracted against the appropriate "blank" mesophase spectra.[39] The amide I and amide II bands were resolved by second-derivative Savitzky−Golay nine-point smoothing function.

2.5. EPR. The 5-DSA probe was first dissolved in chloroform at a concentration of 2.5 × 10^{-3} M as a stock solution. An appropriate quantity of the probe solution was placed in tubes, and the solvent was then evaporated before preparing the mesophases within these tubes. A low concentration of 1 × 10^{-4} M probe in the examined systems was used for all EPR studies. Such a low concentration has already been demonstrated not to perturb similar nanostructures.

The spectra were recorded 24 h after sample preparation. Samples were placed in a 20 mm long, 4 mm outer diameter Wilmad EPR quartz tube. EPR measurements at the temperature of 298.0 K were carried out using a Bruker EMX-220 X-band (ν ∼9.4 GHz) equipped with Bruker ER 4121VT LN2 temperature accessories and Agilent 53150A frequency counter. EPR experiment setup includes a nonsaturating MW power of 20 mW, modulation amplitude of 1 G, MW frequency of 9.42 GHz, center magnetic field of 3355.00 G, sweep width of 200.00 G, resolution of 1024 points, time constant of 0.32 ms, and conversion time of 10.24 ms, with a coherent acquisition of 49 scans per each EPR spectrum.

2.6. *In Vitro* Skin Penetration Study. Na-DFC and CLXB permeability through fresh porcine skin was determined *in vitro* using a Franz diffusion cell system (PermeGear, Inc., Hellertown, PA, USA). Before the experiments, the skin was thawed and mounted on the Franz cells (diffusion area of 0.635 cm^2) with the stratum corneum facing the donor compartments. In the Na-DFC experiments, the receptor compartment was filled with PBS (pH 7.4). In the CLXB experiments, due to the poor aqueous solubility of CLXB, the receptor compartment was filled with 3:7 methanol:PBS (pH 7.4). 100 mg of the formulations containing 1 wt % of Na-DFC or CLXB ("blank") and samples containing 1 wt % Na-DFC or CLXB together with 2 wt % of TAT ("TAT-loaded") were applied to the surface of the stratum corneum. The receptor phase was kept under constant stirring at 37 ± 0.5 °C. The receptor buffer was sampled on fixed times during a 24 h experiment.

2.6.1. Analytical Methods. Na-DFC and CLXB content in the samples was determined on a high-performance liquid chromatograph (HPLC, Waters 600 series) equipped with photodiode array detector (Waters 996) and autosampler (Waters 717 plus) (Waters, Milford, MA, USA). The column used was a Luna 5 μm, C18, 250 mm × 4.6 mm (Phenomenex, Torrance, CA, USA.) The experiments were performed at ambient temperature at a flow rate of 1 mL min^{-1}. The injection volume was 40 μL. In the Na-DFC experiments, isocratic elution was carried out with 35% acetonitrile and 65% water containing trifluoroacetic acid 0.1% (w/v). The wavelength for UV detection was 275 nm, and the retention time was 8 min. In the CLXB experiments, the mobile phase was acetonitrile:water (40:60). Retention time was 6.9 min, and the UV detection was performed at 260 nm wavelength.

2.6.2. Calculation of the in Vitro Data. In the *in vitro* skin penetration trials using Franz cells, because of the sampling from the receiver solution and replacement with equal volumes of buffer, the receiver solution was constantly being diluted. Considering this, the cumulative drug permeation (Q_t) was calculated from eq 1:[40]

$$Q_t = V_r \cdot C_t + \sum_{t=0}^{t-1} V_s \cdot C_i \tag{1}$$

where C_t is the drug concentration of the receiver solution at each sampling time, C_i is the drug concentration of the ith sample, and V_r and V_s are the volumes of the receiver solution and the sample, respectively. The obtained data were expressed as the cumulative drug permeation per unit of skin surface area, Q_t/S. The steady-state fluxes (J_{ss}) were calculated by linear regression interpolation of the experimental data, as shown by eq 2:

$$J_{ss} = \frac{\Delta Q}{\Delta t \cdot S} \tag{2}$$

Apparent permeability coefficients (K_p) were calculated according to eq 3:

$$K_p = \frac{J_{ss}}{C_d} \tag{3}$$

where C_d is the drug concentration in the donor compartment (1 × 10^4 μg mL^{-1}), while assuming that under sink conditions the drug content in the receiver was negligible compared with the drug in the donor. Solvent, water activity, and water gradient were minimum affected under the experimental conditions.

3. RESULTS

3.1. The Solubilization within the Mesophase. The maximal TAT loading level which does not disrupt the hosting cubic mesophase was 5 wt % (29 mM from the total formulation). Increasing TAT content above this threshold seems to be strongly altering the mesophase curvature causing deformation of the cubic system and phase separation. In the lamellar mesophase, TAT maximal loading was only 4 wt % (23 mM). Above this concentration TAT precipitated out of the lamellar systems but, interestingly, the lamellar mesophases remained intact. This difference in the TAT loading capacity of the mesophases might be a result of the composition difference. The cubic system (composed of GMO:ethanol:water weight ratio of 57:5:38) is rich in water (38 wt %) while the lamellar system (composed of GMO:ethanol:water weight ratio of 70:10:20) contains less water (20 wt %) and more GMO. It seems that TAT solubilization in the water channels exhibits significant interactions with hydrophilic domains of the mesophases, and those interactions are more abundant in the cubic more hydrophilic system. The reason might also be geometric: as the cubic system contains larger voids between the tails and the aqueous channels are swollen, the stacked

dx.doi.org/10.1021/jp412739p | J. Phys. Chem. B 2014, 118, 6277−6287

lamellar-planar system is denser and the free spaces are smaller. In the following sections we will try to elucidate the different solubilization patterns and properties of the systems in the presence of TAT.

3.2. SAXS. The SAXS results revealed that, upon loading TAT (alone) in the cubic, as well as in the lamellar, systems, the water channels swell. In the cubic system, increasing levels of solubilized TAT (up to 5 wt %), showed gradual enlargement of the lattice parameter, α, from 115 ± 0.5 Å in the "empty" system to 124 ± 0.5 Å in the system loaded with 5 wt % TAT. Similarly, TAT loading caused a small gradual swelling of the lamellar system from 41 ± 0.2 Å ("empty" system) up to 45 ± 0.3 Å (at 4 wt % TAT). The swelling in both cases might result from the presence of the large, hydrated peptide (M_w = 1717 gr mol^{-1}) which occupies the aqueous cylinders and increases their diameters. One would expect that the hydration of the charged peptide, upon embedment in the system, would dehydrate the GMO headgroups and lead to an apparent shrinkage of the channels ("salting out" of the water from the surfactant), yet it seems that the opposed effect was more pronounced and apparently due to the large dimensions of TAT and the geometric constraints which accompany its solubilization within the nanostructures. This might hint that the gain in free energy, resulting from the headgroup hydration and maintenance of the system curvature, is strong and favorable compared to competition over the free water in the channel interface.

3.3. SD-NMR. For understanding the specific solubilization loci of TAT within the mesophases, SD-NMR study was performed. The self-diffusion coefficients of the mesophase components were determined with the increasing concentrations of solubilized TAT. The deviations between measuring triplicates of each sample did not exceed 4 × 10^{-11} m^2 s^{-1}. We found that in the cubic system TAT binds water and slightly decreases its diffusivity from 8.5 × 10^{-10} to 6.6 × 10^{-10} ± 4 × 10^{-11} m^2 s^{-1} (Figure 1). The diffusivities of TAT itself were

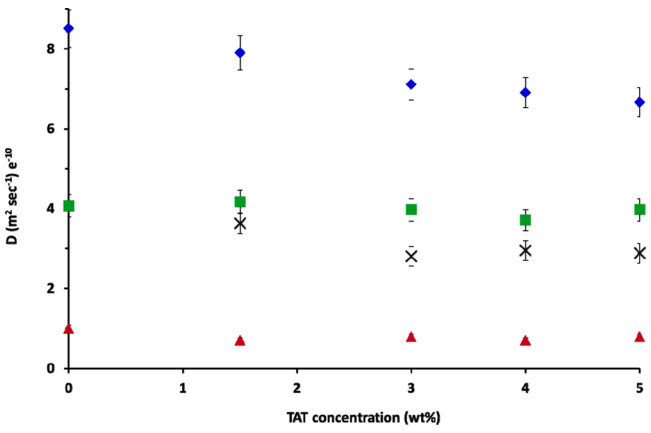

Figure 1. Diffusivities of GMO (red ▲), ethanol (green ■), D_2O (blue ◆), and TAT (×), as affected by TAT loads within the cubic mesophase, at 25 °C.

decreased upon increasing its content in the cubic system, from 3.6 × 10^{-10} to 2.8 × 10^{-10} ± 4 × 10^{-11} m^2 s^{-1} (a decrease of 22%), probably as a result of increased chemical interactions and physical limitations which occur between the peptide and the hosting mesophase. We found that TAT diffusivities are close to those of the ethanol, hinting that both of them might be located at the same region of the mesophase water channels. GMO and ethanol were not affected by the presence of the peptide in the system, as their diffusivities remained constant upon varying TAT content in the system (Figure 1). The high affinity of TAT to water and the majority of charged groups in the peptide strengthen the suggestion that the diffusivities of TAT and the water were slightly decreased due to mutual interactions between them. The calculated diffusion coefficient reflects an average of the diffusivities of the different water populations within the systems. There appears to be a "new" fraction of water which is strongly bound to the charged TAT residues (probably at the expense of the free water which populated the inner channel regions[41]) and comprise lower diffusivity, which is reflected in the average decrease of the water diffusion coefficient. TAT consists of six arginine and two lysine basic amino acids, three polar (uncharged) glutamine and glycine residues, and two hydrophobic proline groups. We should mention the large hydration tendency of the guanidinium arginine residues; the arginine guanidine ion can form up to six hydrogen bonds.[42]

TAT had no significant effect on the diffusivities of the GMO or the ethanol since they remained unchanged, hinting that TAT interaction with GMO and ethanol is not significant (Figure 1). The hydrated TAT seems to be located within the aqueous channel cores.

It is not surprising to find that in both cubic and the lamellar mesophases the water and the ethanol diffuse faster than the large GMO that is immobilized to the bicontinuous interface by hydrogen and van der Waals intermolecular interactions. In contrast, the relatively small water and ethanol molecules populate the inner parts of the cylinders, flow freely, and represent higher diffusivities. In addition, the diffusion coefficients of the lamellar system's components are higher than those of the cubic; this issue was previously reported and can be explained by the very dense packing of the lamellar mesophase, compared to the swollen cubic.[19] The GMO in the stacked-lamellar system forms bilayer lamellae at which the tails are entangled between the layers, the headgroup hydration is limited due to low water content, and the total packing is much denser compared to the cubic phase which exhibits large distances between the domains, swollen micelles due to high water amount, and free voids which arise between the tails at the continuous region, due to the geometrical situation. These chemical and geometrical factors result in diffusivity differences between the mesophases.

TAT loading in the dense, lamellar system resulted in a slight decrease in water diffusivity, similarly to the cubic system, yet, at TAT loads higher than 2 wt %, the water diffusivity was no longer affected by TAT content, indicating that TAT high loads had no apparent effect on the water diffusivity. In these loading levels we detected equal diffusivities of TAT and GMO (Figure 2). It seems that, at the high TAT loads, the dense packing or the chemical composition of the lamellar system forces TAT peptide to hydrogen-bond to the GMO hydroxyls.

We suggest that each of the mesophases dictates different solubilization patterns and loads as well as different water managements within the water channels and solubilization loci of the TAT peptide. In the swollen cubic mesophase, which is rich in water and contains large aqueous channels, TAT is located inside the channel cores and is highly hydrated due to binding to the "free" water which populates the channel cores. Its diffusivities are 2.5−3 times lower than those of the water and are close to those of the ethanol, suggesting that, similarly to the ethanol, TAT can flow through the channels with some

dx.doi.org/10.1021/jp412739p | J. Phys. Chem. B 2014, 118, 6277−6287

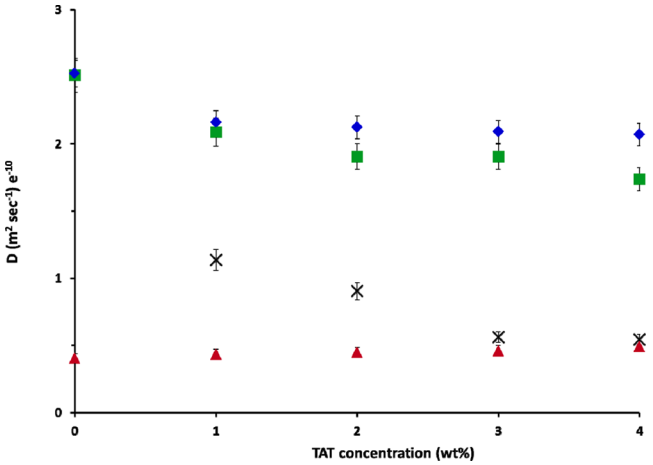

Figure 2. GMO (red ▲), ethanol (green ■), D_2O (blue ◆), and TAT (×) diffusivities, as affected by TAT concentration within the lamellar mesophase, at 25 °C.

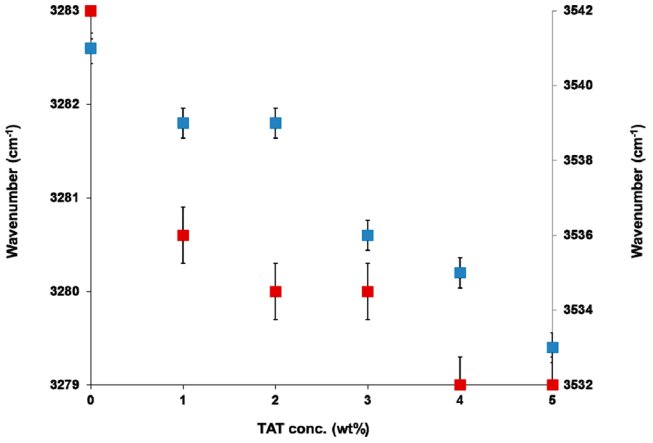

Figure 3. Vibration modes of the "bound" water (red, left *Y* axis) and the "free" water (blue, right *Y* axis) as affected by TAT loads in the cubic mesophase.

restrictions due to the channel dimensions, and to weak interactions with the GMO. In the lamellar system, TAT diffusivities are 3−4 times lower than in the cubic phase. Its solubilization is accompanied by water binding, yet at high concentrations TAT seems to populate alternative solubilization sites, closer to the GMO headgroups which bind it and stabilize its solubilization. We can suggest that the cubic system contains an excess of water molecules, free to hydrate TAT peptide, and to enable its solubilization (and free flow) within the aqueous channels cores, while in contrast, the lamellar system has almost half the amount of water, and contains more GMO, forcing the high concentrations of the peptide to be solubilized within the channel "walls", and to be adsorbed on the surfactant headgroups. This difference might explain the low diffusion coefficients of TAT loads in the lamellar system, which are close to those of the GMO (see also sections 3.4, 3.5, and 3.6). This suggestion will be examined in the following sections.

3.4. ATR-FTIR Study: TAT Effect on the Mesophase. For understanding the specific solubilization loci of TAT within the mesophases, ATR-FTIR experiments were performed. The mesophases reveal characteristic infrared vibration modes representing the different regions. A detailed discussion of this set of analysis is described elsewhere.[43,44] The hydrophilic region is represented by the water and the GMO O−H headgroups. The water population in nanostructured systems can be either "free" or "bound". These different states of water can be detected macroscopically by DSC measurements, upon identification of the various melting events of the water, as "free" water melts at 0 °C while "bound" water melts at lower temperatures. These different states of matter can be also detected microscopically by their absorbance of IR energy; typically "bound" water absorb energies at lower wavenumbers, compared to "free" water, due to the limitations on vibration of this species as a result of strong binding to the surroundings. Any increase in water binding, as an effect of a guest molecule, will alter the water melting point (detected by DSC) and vibration modes detected by FTIR.[45−48]

In the cubic system, TAT loading (up to 5 wt %) affected the vibration modes of both the "bound" and "free" water populations[49,50] and decreased them gradually from 3283 and 3541 cm^{-1} to 3279 and 3458 cm^{-1}, respectively (Figure 3), hinting that the water is strongly bound in the presence of the hydrated TAT. This observation is in good agreement with the SD-NMR results, which showed enhanced water binding upon increasing TAT loading. At the interfacial mesophase region, TAT had no significant effect on the vibration frequency of the different groups including the carbonyl and the ester absorbance; TAT had no effect on the GMO tails, either, hinting that the peptide has no significant interaction with the lipophilic mesophase regions.

Interestingly, in the lamellar system, similar water binding was apparent at low TAT concentrations, up to 2 wt %, yet, at higher TAT loads, no additional effect was detected on the water, but the GMO γ-OH group revealed enhanced binding as its vibration mode was shifted from 1051 to 1047 cm^{-1}. In addition, in the lamellar system there was an apparent shift of the GMO "free" and "bound" carbonyl vibration modes from 1749 and 1729 cm^{-1} to lower wavenumbers (1747 and 1725 cm^{-1}, respectively), indicating more interactions and enhanced binding between the GMO C═O groups and their surroundings, hinting an effect of the peptide on this region. The tails were not affected by TAT, similarly to the situation in the cubic phase. These findings strengthen the suggestion that TAT in the cubic mesophases is solubilized in the core of each channel while in the lamellar system a GMO−TAT interaction is essential to guarantee high solubilization loads; GMO is involved with the solubilization which occurs via an interaction with the headgroups. The effects of the different solubilization sites on TAT secondary structures and on the drug release rates from the mesophases will be explored in the following sections (sections 3.5 and 3.6).

3.5. ATR-FTIR Investigation of TAT Structure. ATR-FTIR spectroscopy is a useful technique providing valuable information on protein and peptide secondary structures.[51] Vass et al.[52] and Kong et al.[53] published important reviews concerning the identification of different protein and peptide structural motifs, according to their typical vibration modes in the IR region. The peptide backbone groups absorb specific energies corresponding to the hydrogen bond lengths, derived from the different secondary structures which they form. There are characteristic vibration modes and patterns representing every structure, including α-helices, β-sheets, β- and γ-turns, random coils, and more. There are a few characteristic bands representing the peptide backbone, including the amide A, between 3460 and 3410 cm^{-1}, and 3380−3300 cm^{-1}, resulting

dx.doi.org/10.1021/jp412739p | J. Phys. Chem. B 2014, 118, 6277−6287

from N−H stretching for "free" or "hydrogen-bonded" groups, respectively. The amide I band between 1695 and 1610 cm^{-1} reflects the C═O stretching with N−H and C−H stretch; the acceptor carbonyl absorbs at 1645−1635 cm^{-1} as the donor amide group vibrations occur at 1690−1660 cm^{-1}. Characteristically, for β-sheets the ratio between these vibration intensities is 1:10−1:8, while for β-turns it is 1:2−2:3, as derived from the ratio between the different carbonyl populations.[52] Proton donor solvents may shift the amide I band of the first acceptor carbonyl to lower wavenumbers below 1635 cm^{-1}. Helical structures have typical vibration modes occurring at 1660−1645 cm^{-1}. Random coils have characteristic infrared band between 1640 and 1648 cm^{-1}. The amide vibrations are highly sensitive to H-bonding; a change in hydrogen bonding distance of 0.002 Å will shift the wavenumber of the peptide amide band by approximately 1 cm^{-1}. The amide II band, occurring at 1575−1480 cm^{-1}, results from N−H bending coupled with C−N stretching. Strong H-bonds shift the amide II band toward lower wavenumbers, and *vice versa*.

TAT amide I band (Figure 4A) revealed that the peptide in solution is basically composed of a random coil and a fraction

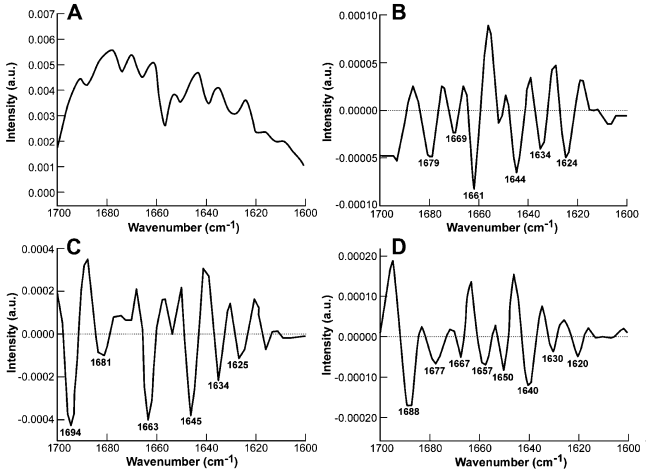

Figure 4. (A) Typical amide I band of TAT peptide in aqueous solution (20 mM). (B−D) Second derivative FTIR spectra of TAT: (B) in aqueous solution (20 mM), (C) solubilized in the cubic mesophase (4 wt %, 23 mM), and (D) solubilized in the lamellar mesophase (4 wt %, 23 mM). The patterns were identical for all TAT concentrations within each mesophase.

of characteristic β-turns. The second-derivative ATR-FTIR amide I spectrum of TAT in water (Figure 4B) reveals typical vibration modes of the β-turns at 1661 and 1634 cm^{-1} with the ratio of 2:1 between them. Also the vibration modes at 1669 and 1679 cm^{-1} can be related to this structural motif.[53] The intense vibration mode at 1644 cm^{-1} can result from a random coil structure while the absorbance at 1624 cm^{-1} might be attributed to the proline residues. Upon embedding TAT into the cubic mesophase, the structural motifs were conserved, yet they experienced some slight shifts (Figure 4C). The dominant random coil vibration mode at 1644 cm^{-1} was conserved as well as the absorbance of the β-turns at 1634 and 1663 cm^{-1}. Interestingly, the vibrations at 1669 and 1679 cm^{-1}, characteristic of β-turns, were shifted to higher wavenumbers, 1681 and 1694 cm^{-1}, also characteristic of β-turns,[54,55] hinting probably that the structure was conserved yet the bond lengths are longer, and peptide folding occurs in a "looser" way. In other words, the embedment of the peptide within the cubic mesophase conserves its structure, which is composed of a fraction of β-turns connecting the random coil domains.

When considering TAT embedment within the lamellar system (Figure 4D), the general pattern seems unchanged as the vibration modes were conserved, yet, many vibration modes were shifted to lower wavenumbers, including the proline absorbance (1624 → 1620 cm^{-1}), the random coil absorbance (1644 → 1640 cm^{-1}), and some β-turn vibrations (1661 → 1657 and 1634 → 1630 cm^{-1}). The proline shift might hint that in the lamellar phase it experiences a more hydrophobic medium, compared to the aqueous environment. The shifts of the random coil and the β-turns suggest that in the lamellar system the hydrogen bond lengths are shorter and the peptide folding is denser, compared to the aqueous solution and to the cubic system. The absorbance at 1688 cm^{-1} hints a "new" population of β-turns, resembling the 1694 cm^{-1} vibration mode which appeared in the cubic system, implying that, when embedded within the nanostructured mesophases, the peptide adopts unique folding which exhibits shorter distances in the lamellar system, compared to the swollen cubic. It seems that the dense packing and smaller aqueous channels in the lamellar system create a geometrical constraint which forces TAT peptide to fold in a denser assembly.

The suggestion that TAT adopts a more compact folding when embedded in the lamellar system is strengthened by the peptide amide II spectra between the peptide spectrum in the mesophases. The characteristic vibration modes of the peptide at the cubic system were shifted toward lower wavenumbers, when embedded in the lamellar system (Figure 5), hinting on shorter hydrogen bonds lengths and denser folding state.[52]

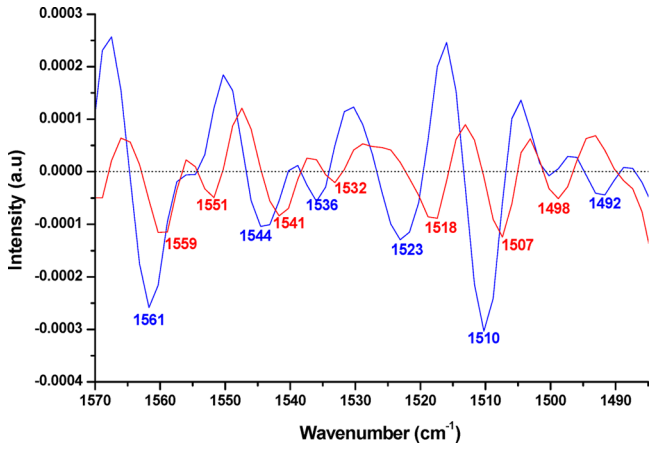

Figure 5. Second derivative amide II band of TAT peptide solubilized in the cubic mesophase (blue) and in the lamellar mesophase (red) (4 wt %, 23 mM).

Several investigations[56,57] concerning HIV-TAT secondary structure revealed by NMR and molecular dynamics simulations that the peptide in solution is basically arranged as a highly dynamic random coil stabilized by hydrogen bonds with the water. TAT comprises high mobility through lipid bilayers, due to high affinity to the membranes, which is 80% electrostatic and 20% hydrophobic. In addition, hydrogen bonds play a key role in TAT binding to the membrane; the arginine guanidine N−H binds to the membrane phosphate P−O group as each guanidine ion can bind up to five phosphate

dx.doi.org/10.1021/jp412739p | J. Phys. Chem. B 2014, 118, 6277−6287

molecules. The combination of the electrostatic, hydrophobic, and hydrogen bond effects facilitate TAT insertion into the glycerol backbone of the membrane−water interface.[58] TAT insertion into the living cell membrane is extremely rapid, as it relies on transient interactions of the arginine residues with the membrane phosphate groups. The peptide does not cause any transparent damage to the membrane but may cause transient defects due to the guanidine−phosphate bonds.[59]

Remarkably, when simulating TAT penetration into a cell, TAT remains a random coil also upon insertion into the lipid bilayer,[58] probably due to substituting the hydrogen bonds with the water by intermolecular bonds with the lipid phosphates, and by residing in the lipid−aqueous interface. The random coil structure of TAT and another CPP, penetratin, suggests that the lack of amphipathic structure is essential for rapid translocation of these arginine-rich CPPs across the lipid membrane without causing permanent damages to the membrane integrity. The membrane−glycerol region has intermediate dielectric constant and accommodates TAT through the polar phosphate and carboxyl groups, which can act as hydrogen bond acceptors for the guanidine. Interestingly, crystallographic studies showed that aqueous solutions of phospholipids with TAT undergo a phase transition from a lipid bilayer to a *Pn*3*m* double-diamond phase, where the lipid molecules surround large, 6 nm water pores.[60] We can suggest that the high structural flexibility of TAT, in addition to its tendency to bind to lipid headgroups and to be involved in creating lipid self-assemblies, might explain its behavior in the lamellar phase, as it substitutes the hydrogen bonds with water by bonds to the GMO headgroups, and adopts special folding around them, similarly to its interaction with the cell membranes. The following EPR measurements (section 3.6) will attend to examine and compare the microenvironment in the cubic and lamellar mesophase interfaces with the presence of TAT.

3.6. EPR Study. Electron paramagnetic resonance spectroscopy is a sensitive method for the characterization of nanostructured systems.[61] The spin probe, a stable nitroxide radical, 5-DSA, was inserted into the lamellar and the cubic mesophases at the stage of their preparation, and the EPR spectra were computed by means of the computation procedure of Budil et al.[62] to extract the following parameters: (i) the average value of the A_{ii} components for the hyperfine coupling between the electron spin and the nitrogen nuclear spin ($\langle A_N \rangle = (A_{xx} + A_{yy} + A_{zz})/3$), indicative of the environmental micropolarity around the probe, (ii) τ, the correlation time for the rotational diffusion motion, representing the microviscosity of the system at the nitroxide site, and (iii) S, the order parameter of the hosting mesophase. Higher degree of order in the system strongly hinders the probe mobility, and *vice versa*. S values may vary between $S = 0$, for a completely disordered system, and $S = 1$, for an ordered one. The cumulative (both experimental and calculations) error of the EPR parameter determination does not exceed 2.5%.

The EPR spectra, on the basis of the simulation parameters reported in Table 1 in the Supporting Information, reveal interesting results. In the cubic system, TAT loading up to 4 wt % slightly increased the system order (S), yet it did not cause any significant effect on the microviscosity (τ) or micropolarity ($\langle A_N \rangle$), probably due to its location in the aqueous channel cores, not affecting the lipophilic probe which is embedded at the interface. High TAT load of 5 wt % decreased the microviscosity and increased the polarity (Table 1 in the Supporting Information). At this high concentration the TAT effect was noticeable also at the interface region as the TAT reached the GMO and affected it to become more polar and less densely packed, probably also as a result of the swelling revealed by SAXS. Once higher amounts (above 5 wt %) of TAT were incorporated into the cubic mesophase, the microviscosity immediately dropped, the order parameter was zero, and a fast collapse of the cubic structure was observed. This observation can support the SAXS result which showed perturbation of the cubic microstructure which occurs above this concentration.

In the lamellar system, TAT gradually increased the order degree and the microviscosity, after an initial small decrease at 1 wt % (Table 1 in the Supporting Information). Also the micropolarity was increased with the presence of the hydrophilic peptide in the interface. These effects hint that the probe microenvironment in the interface is more ordered, dense, and viscous, and comprises some more polarity, with the presence of TAT. It seems that the peptide is incorporated at the interface and leads to the creation of more bonds between the lamellar system components, and to increase the system tendency to densely self-assemble into the nanostructured state.

The EPR findings correspond to the former SD-NMR and the ATR-FTIR results which suggested different manners of TAT solubilization in the cubic and the lamellar systems. In the water-rich cubic phase, TAT populates the water channel cores and binds mainly water molecules, thus its interaction with GMO (revealed by ATR-FTIR and EPR) is minimal, and its diffusion coefficient of flowing through the channels is relatively high. In contrast, TAT solubilization in the lamellar phase occurs also by binding to the GMO and their diffusion coefficients are close to each other. The effect of TAT on the interface region was revealed by ATR-FTIR and EPR, which showed increased binding with the presence of the peptide and an enhancement of the order degree and the microviscosity as TAT was associated with the lamellar system interfacial interactions. The structural investigation showed that, when embedded at the lamellar phase, TAT reveals denser packing and a more compact folding, with higher fraction of β-turns, compared to its state in the cubic system and the aqueous solution. It seems that the low water amount and the dense packing within the lamellar system force TAT peptide to rearrange in a different folding state as a reason for the environmental constraints. This kind of behavior is common to different RNA-binding protein domains which fold differently upon binding to RNA[63] as in some cases the RNA serves as the folding scaffold and was reported to occur also in TAT.[64] We can suggest that, in the lamellar system, the situation might resemble this behavior as TAT binding to GMO leads to its compact folding around the GMO headgroups. The next section (section 3.7) will examine how the different solubilization states of TAT within the mesophases affect the drug release kinetics.

3.7. TAT Effect on the Skin Permeation. This research is mainly focusing on developing formulations for controlled skin delivery of the water-insoluble Na-DFC and CLXB. The cubic and the lamellar mesophases serve as the gel matrix (carrier) of the drugs, designated to be rubbed on the skin. For enabling controlled delivery, TAT was added to the mesophases, and its effect on NSAID diffusion through porcine skin was evaluated. TAT, which is a very effective membrane penetrating peptide, was examined as a skin penetration enhancer, in order to overcome the stratum corneum barrier for enhanced NSAID

dx.doi.org/10.1021/jp412739p | J. Phys. Chem. B 2014, 118, 6277−6287

delivery. The transdermal delivery was examined using Franz diffusion cells as the porcine skin was mounted over a diffusion cell filled with PBS. 100 mg of "blank" formulations, containing 1 wt % of Na-DFC or CLXB only, and "combined" formulations, containing Na-DFC and TAT, or CLXB and TAT (1 wt % of the drug and 2 wt % of TAT), were rubbed on the stratum corneum surface. The buffer under the skins was sampled every few hours, and the amount of drug which diffused to it was quantized by HPLC.

When examining the skin permeation of Na-DFC, slight differences were observed between the diffusion rates of the drug from the "blank" lamellar and cubic mesophases. The permeation patterns over the whole time range were almost identical. In previous investigations of Na-DFC diffusion through PESU membranes, the cubic systems released higher Na-DFC amounts than the lamellar, suggesting that when skin permeation is examined, the mesophase nanostructure and water amount are not the major factors influencing the diffusion rate.[19] It seems that the release experiments through the artificial PESU membranes examine the first steps of the drug diffusion through the mesophase and out of it, toward an acceptor buffer, while the skin permeation experiments include the competitive interaction with the skin, which is a biologically dense barrier and strongly controls the permeation rates. The previous and the present results suggest that the skin interaction seems to be the rate-determining step and is a crucial phase, in addition to the steps of the drug diffusion within the mesophases and the migration out of it.

The presence of TAT in the mesophases remarkably affected Na-DFC skin permeation from the cubic system. A noticeable TAT effect was apparent from the seventh hour onward, and it grew larger with time, until the overall amount of Na-DFC which penetrated through the skin was 6-fold higher compared to the blank cubic system (Figure 6A).

The TAT effect on Na-DFC penetration from the lamellar system was much smaller; a slight increase of Na-DFC diffusion was apparent only after the 18th hour onward, and the total amount which penetrated through the skin was 1.8 higher than at the "blank" lamellar system. It seems that the TAT effect on the skin permeation is more limited when embedded at the lamellar system. The slope of the permeation curves at steady state enables the calculation of K_p, the permeability coefficients, indicative of the diffusion rates at each system. K_p was calculated according to the linear region, based on the cumulative permeation curve usually from the fifth or the sixth hour onward, due to a "lag time" which it takes for the drug to accumulate on the outer skin surface and to penetrate in a constant manner. The regression lines used for the calculations are of minimum $R^2 = 0.95$. K_p was 6.6-fold higher in the TAT-loaded cubic system, compared to the blank (Figure 6B). In the lamellar system, the TAT effect was quite minor and K_p enhancement was only 1.3-fold.

When examining CLXB diffusion, one can notice that the tendency of CLXB to migrate out of the mesophases and through the skin is much smaller than that of Na-DFC. The permeability coefficients of the blank systems, containing drug only, were 5- and 8.5-fold lower for CLXB cubic and lamellar systems, compared to the Na-DFC ones, respectively. Similarly to Na-DFC, also the diffusion curves of CLXB blank systems were identical, and no apparent difference of CLXB diffusion was revealed between the blank cubic and lamellar systems (Figure 7A).

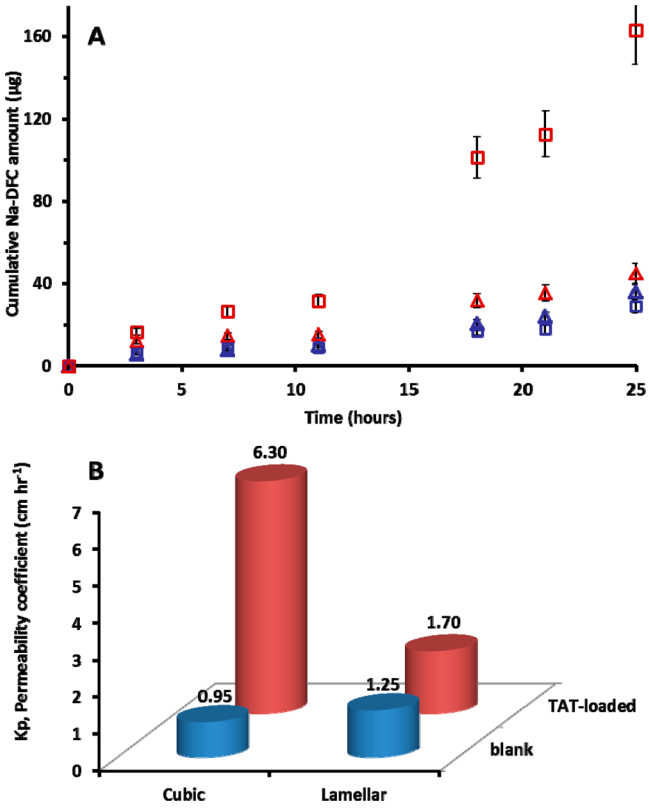

Figure 6. (A) The cumulative Na-DFC amount which penetrated through the skin from the lamellar (Δ) and cubic (■) blank (blue) and TAT-loaded (red) systems. (B) K_p, the permeability coefficients of Na-DFC diffusion through the skin, from the blank (blue) and the TAT-loaded (red) cubic and lamellar systems.

TAT enhanced CLXB skin permeation from the cubic mesophase to a noticeable extent. Its effect was apparent from the eighth hour onward, and the total CLXB amount which penetrated the skin was 8 times higher, compared to the blank cubic system. The TAT effect on the diffusion from the lamellar mesophase was very small; an apparent 1.5-fold difference was revealed after 20 h (Figure 7A). TAT behavior was analogous in the Na-DFC and the CLXB systems: a significant enhancement of the diffusion from the cubic systems and a small, delayed effect on the diffusion from the lamellar.

The calculation of K_p, the permeability coefficients, revealed that the CLXB skin permeation rate enhancement was 9-fold in the cubic system, and 1.7-fold in the lamellar (Figure 7B).

We can conclude that TAT can serve as an efficient skin penetration enhancer for Na-DFC and CLXB, from cubic mesophases. The presence of the peptide in the system significantly accelerates the skin permeation rate of the drugs and increases the total amounts of drugs which penetrate through the skin. In contrast, in the lamellar system the TAT effect is small, probably due to increased binding of TAT to the GMO and to low diffusion coefficients which slow TAT migration toward the skin and limit its noticeable effect. This result demonstrates the strong importance of choosing the appropriate hosting mesophase which can provide the ultimate matrix for drug solubilization and diffusion, and for efficient use of the permeation enhancer.

dx.doi.org/10.1021/jp412739p | J. Phys. Chem. B 2014, 118, 6277−6287

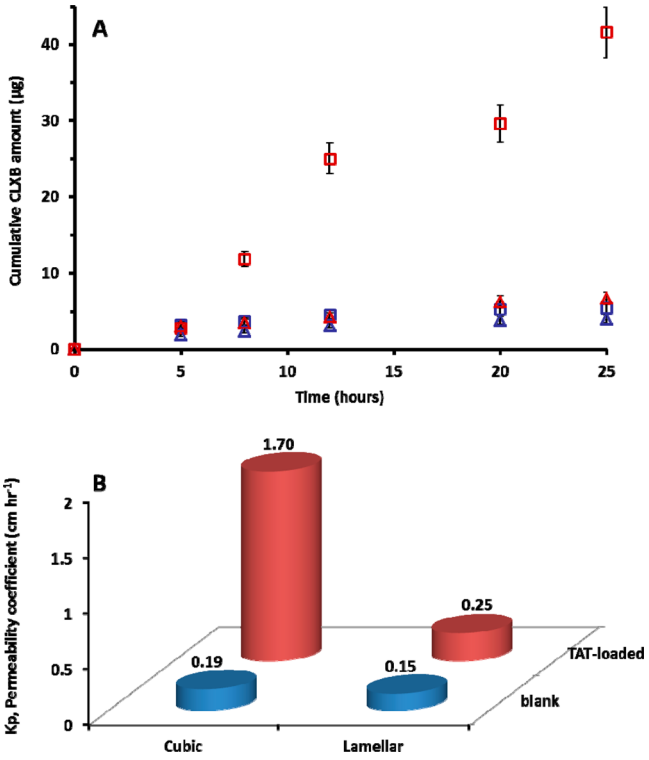

Figure 7. (A) The cumulative CLXB amount which penetrated through the skin from the lamellar (Δ) and cubic (■) blank (blue) and TAT-loaded (red) systems. (B) K_p, the permeability coefficients of CLXB from the blank (blue) and the TAT-loaded (red) cubic and lamellar systems.

4. DISCUSSION AND CONCLUSIONS

TAT swells the cubic and lamellar mesophases when embedded into them, probably due to enlargement of the distances between the GMO domains. SD-NMR measurements revealed that, in the cubic phase, TAT is bound to the water and flows freely, yet in the lamellar phase, TAT is bound to the GMO and its movement is restricted. It seems that, due to the composition and geometrical differences between the systems, in the lamellar phase GMO is involved in TAT solubilization. ATR-FTIR measurements support this suggestion, revealing that in the cubic phase TAT binds mainly the water while in the lamellar system TAT strongly affects the GMO γ-OH headgroups and carbonyls. Second-derivative ATR-FTIR studies of TAT amide I revealed that its insertion into the cubic mesophase conserves its random coil structure which contains some β-turns while in the lamellar system the structural motifs exhibited shorter bond lengths, hinting compact folding of the peptide within the lamellar system upon binding to GMO. TAT amide II spectra strengthened this suggestion, revealing that TAT structure in the cubic phase corresponds to its structure in aqueous solution, but in the lamellar phase shorter H-bonds imply denser folding. The EPR study showed that TAT influenced the interfacial regions of the lamellar system, suggesting that the peptide populates the interface and enhances the internal binding. In the cubic phase, TAT embedment in the aqueous cores had on effect on the interface.

TAT enhanced the skin permeation of both Na-DFC and CLXB to a remarkable extent, exclusively from the cubic mesophases; the effect on drug diffusion from the lamellar systems was low. The difference might result from the finding of specific binding between TAT and GMO in the lamellar system, decreased diffusion coefficients of the peptide within the lamellar system, compared to the cubic one, and delayed movement toward the skin. TAT was found to be a very effective *penetration enhancer* for transdermal delivery of Na-DFC and CLXB from cubic mesophases. It increased their diffusion rates in factors of 6- and 9-fold, respectively, and enlarged the total quantity which penetrated through the skin. There is a strong dependence of TAT enhancement in the hosting mesophase symmetry, implying the importance of choosing an appropriate mesophase as the release matrix. The specific mechanism of TAT action is interesting and might be derived either from enhanced mobility of the drugs through the mesophase or from specific interactions between TAT and the skin. However, TAT might be utilized as a skin penetrating agent for drugs, and the different characteristics of the solubilization in the mesophases can be further developed for controlling the drug diffusion rated as needed.

■ ASSOCIATED CONTENT

Ⓢ Supporting Information

Table of correlation time for the rotational diffusion motion, isotropic hyperfine coupling between the electron spin and the nitrogen nuclear spin, and order parameter. Complete refs 16 and 29. This material is available free of charge via the Internet at http://pubs.acs.org.

■ AUTHOR INFORMATION

Corresponding Author

*Tel: +972-2-658-6574/5. Fax: +972-2-652-0262. E-mail: garti@vms.huji.ac.il.

Notes

The authors declare no competing financial interest.

The results presented in this manuscript are part of M.C.A.'s dissertation as a partial fulfillment of the requirements toward Ph.D. degree in Applied Chemistry from The Hebrew University of Jerusalem, Israel.

■ ACKNOWLEDGMENTS

We thank cordially Ian Gleaner from the University of Maryland for his great contribution on the skin permeation experiments. We thank the Ministry of Science and Technology for the important and generous Grant # 0398541, which enabled the research.

■ REFERENCES

(1) Engblom, J. Bicontinuous Cubic Phase: A Model for Investigating the Effects on a Lipid Bilayer due to a Foreign Substance. *Chem. Phys. Lipids* **1996**, *84*, 155−164.

(2) Nguyen, T. H.; Hanley, T.; Porter, C. J. H.; Boyd, B. J. Nanostructured Liquid Crystalline Particles Provide Long Duration Sustained-Release Effect for a Poorly Water Soluble Drug After Oral Administration. *J. Controlled Release* **2011**, *153*, 180−186.

(3) Tarafdar, P. K.; Reddy, S. T.; Swamy, M. J. Effect of Hofmeister Series Anions on the Thermotropic Phase Behavior of Bioactive O-Acylcholines. *J. Phys. Chem. B* **2013**, *117*, 9900−9909.

(4) Helledi, L. S.; Schubert, L. Release Kinetics of Acyclovir from a Suspension of Acyclovir Incorporated in a Cubic Phase Delivery System. *Drug Dev. Ind. Pharm.* **2001**, *27*, 1073−1081.

(5) Lee, K. W. Y.; Nguyen, T. H.; Hanley, T.; Boyd, B. J. Nanostructure of Liquid Crystalline Matrix Determines *In Vitro* Sustained Release and *In Vivo* Oral Absorption Kinetics for Hydrophilic Model Drugs. *Int. J. Pharm.* **2009**, *365*, 190−199.

(6) Bitan-Cherbakovsky, L.; Libster, D.; Aserin, A.; Garti, N. Complex Dendrimer-Lyotropic Liquid Crystalline Systems: Structural Behavior and Interactions. *J. Phys. Chem. B* **2011**, *115*, 11984−11992.
(7) Nunes, C.; Brezesinski, G.; Lima, J.; Reis, S.; Lucio, M. Synchrotron SAXS and WAXS Study of the Interactions of NSAIDs with Lipid Membranes. *J. Phys. Chem. B* **2011**, *115*, 8024−8032.
(8) Efrat, R.; Shalev, D. E.; Hoffman, R. E.; Aserin, A.; Garti, N. Effect of Sodium Diclofenac Loads on Mesophase Components and Structure. *Langmuir* **2008**, *24*, 7590−7595.
(9) Amar-Yuli, I.; Aserin, A.; Garti, N. Solubilization of Nutraceuticals into Reverse Hexagonal Mesophases. *J. Phys. Chem. B* **2008**, *112*, 10171−10180.
(10) Achrai, B.; Libster, D.; Aserin, A.; Garti, N. Solubilization of Gabapentin into H-II Mesophases. *J. Phys. Chem. B* **2011**, *115*, 825−835.
(11) Amar-Yuli, I.; Wachtel, E.; Shalev, D. E.; Aserin, A.; Garti, N. Low Viscosity Reversed Hexagonal Mesophases Induced by Hydrophilic Additives. *J. Phys. Chem. B* **2008**, *112*, 3971−3982.
(12) Hawkey, C. J. COX-1 and COX-2 Inhibitors. *Best Pract. Res., Clin. Gastroenterol.* **2001**, *15*, 801−820.
(13) Pereira-Leite, C.; Nunes, C.; Lima, J.; Reis, S.; Lucio, M. Interaction of Celecoxib with Membranes: The Role of Membrane Biophysics on its Therapeutic and Toxic Effects. *J. Phys. Chem. B* **2012**, *116*, 13608−13617.
(14) Hirano, A.; Kameda, T.; Arakawa, T.; Shiraki, K. Arginine-Assisted Solubilization System for Drug Substances: Solubility Experiment and Simulation. *J. Phys. Chem. B* **2010**, *114*, 13455−13462.
(15) Shakeel, F.; Baboota, S.; Ahuja, A.; Ali, J.; Shafiq, S. Skin Permeation Mechanism and Bioavailability Enhancement of Celecoxib from Transdermally Applied Nanoemulsion. *J. Nanobiotechnol.* **2008**, *6*, 8−18.
(16) Singh, G.; Fort, J. G.; Goldstein, J. L.; Levy, R. A.; Hanrahan, P. S.; Bello, A. E.; Andrade-Ortega, L.; Wallemark, C.; Agrawal, N. M.; Eisen, G. M.; et al. G. Celecoxib Versus Naproxen and Diclofenac in Osteoarthritis Patients: SUCCESS-I Study. *Am. J. Med.* **2006**, *119*, 255−266.
(17) Yariv, D.; Efrat, R.; Libster, D.; Aserin, A.; Garti, N. *In Vitro* Permeation of Diclofenac Salts from Lyotropic Liquid Crystalline Systems. *Colloids Surf., B* **2010**, *78*, 185−192.
(18) Giri, A.; Bhowmick, M.; Pal, S.; Bandyopadhyaya, A. Polymer Hydrogel from Carboxymethyl Guar Gum and Carbon Nanotube for Sustained Trans-Dermal Release of Diclofenac Sodium. *Int. J. Biol. Macromol.* **2011**, *49*, 885−893.
(19) Cohen-Avrahami, M.; Shames, A. I.; Ottaviani, M. F.; Aserin, A.; Garti, N. On the Correlation Between the Structure of Lyotropic Carriers and the Delivery Profiles of two Common NSAIDs. *Colloids Surf. B*, DOI: 10.1016/j.colsurfb.2014.04.026.
(20) Frankel, A. D.; Pabo, C. O. Cellular Uptake of the TAT Protein from Human Immunodeficiency Virus. *Cell* **1988**, *55*, 1189−1193.
(21) Heitz, F.; Morris, M. C.; Divita, G. Twenty Years of Cell-Penetrating Peptides: from Molecular Mechanisms to Therapeutics. *Br. J. Pharmacol.* **2009**, *157*, 195−206.
(22) Bahnsen, J. S.; Franzyk, H.; Sandberg-Schaal, A.; Nielsen, H. M. Antimicrobial and Cell-Penetrating Properties of Penetratin Analogs: Effect of Sequence and Secondary Structure. *Biochim. Biophys. Acta, Biomembr.* **2013**, *1828*, 223−232.
(23) Futaki, S.; Goto, S.; Suzuki, T.; Nakase, I.; Sugiura, Y. Structural Variety of Membrane Permeable Peptides. *Curr. Protein Pept. Sci.* **2003**, *4*, 87−96.
(24) Kubiak-Ossowska, K.; Burley, G.; Patwardhan, S. V.; Mulheran, P. A. Spontaneous Membrane-Translocating Peptide Adsorption at Silica Surfaces: A Molecular Dynamics Study. *J. Phys. Chem. B* **2013**, *117*, 14666−14675.
(25) Futaki, S. Arginine-Rich Peptides: Potential for Intracellular Delivery of Macromolecules and the Mystery of the Translocation Mechanisms. *Int. J. Pharm.* **2002**, *245*, 1−7.
(26) Boudier, C.; Storchak, R.; Sharma, K. K.; Didier, P.; Follenius-Wund, A.; Muller, S.; Darlix, J. L.; Mely, Y. The Mechanism of HIV-1 Tat-Directed Nucleic Acid Annealing Supports its Role in Reverse Transcription. *J. Mol. Biol.* **2010**, *400*, 487−501.
(27) Vitagliano, L.; Fiume, G.; Scognamiglio, P. L.; Doti, N.; Cannavo, R.; Puca, A.; Pedone, C.; Scala, G.; Quinto, I.; Marasco, D. Structural and Functional Insights into I kappa B-alpha/HIV-1 Tat Interaction. *Biochimie* **2011**, *93*, 1592−1600.
(28) Rao, G. S.; Siddiqui, M. I.; Arora, S. Molecular Modeling of the HIV-1 TAT Protein - TAR RNA Complex and the Design of an Inhibitor of the Tat/TAR RNA Interaction. *J. Biomol. Struct. Dyn.* **2000**, 65−74.
(29) Devadas, K.; Boykins, R. A.; Hardegen, N. J.; Philp, D.; Kleinman, H. K.; Osa, E. O.; Wang, J.; Clouse, K. A.; Wahl, L. M.; Hewlett, I. K.; Rappaport, J.; Yamada, K. M.; Dhawan, S. S. Selective Side-Chain Modification of Cysteine and Arginine Residues Blocks Pathogenic Activity of HIV-1-Tat Functional Peptides. *Peptides* **2006**, *27*, 611−621.
(30) Katayama, S.; Nakase, I.; Yano, Y.; Murayama, T.; Nakata, Y.; Matsuzaki, K.; Futaki, S. Effects of Pyrenebutyrate on the Translocation of Arginine-Rich Cell-Penetrating Peptides Through Artificial Membranes: Recruiting Peptides to the Membranes, Dissipating Liquid-Ordered Phases, and Inducing Curvature. *Biochim. Biophys. Acta, Biomembr.* **2013**, *1828*, 2134−2142.
(31) Meade, B. R.; Dowdy, S. F. Exogenous siRNA Delivery Using Peptide Transduction Domains/Cell Penetrating Peptides. *Adv. Drug Delivery Rev.* **2007**, *59*, 134−140.
(32) Kawamura, K. S.; Sung, M.; Bolewska-Pedyczak, E.; Gariepy, J. Probing the Impact of Valency on the Routing of Arginine-Rich Peptides into Eukaryotic Cells. *Biochemistry* **2006**, *45*, 1116−1127.
(33) Wender, P. A.; Mitchell, D. J.; Pattabiraman, K.; Pelkey, E. T.; Steinman, L.; Rothbard, J. B. The Design, Synthesis, and Evaluation of Molecules that Enable or Enhance Cellular Uptake: Peptoid Molecular Transporters. *Proc. Natl. Acad. Sci. U.S.A.* **2000**, *97*, 13003−13008.
(34) Vives, E. Cellular Uptake of the Tat Peptide: an Endocytosis Mechanism Following Ionic Interactions. *J. Mol. Recognit.* **2003**, *16*, 265−271.
(35) Wu, Z.; Cui, Q.; Yethiraj, A. Why Do Arginine and Lysine Organize Lipids Differently? Insights from Coarse-Grained and Atomistic Simulations. *J. Phys. Chem. B* **2013**, *117*, 12145−12156.
(36) Hu, Y.; Ou, S. C.; Patel, S. Free Energetics of Arginine Permeation into Model DMPC Lipid Bilayers: Coupling of Effective Counterion Concentration and Lateral Bilayer Dimensions. *J. Phys. Chem. B* **2013**, *117*, 11641−11653.
(37) Manosroi, J.; Lohcharoenkal, W.; Gotz, F.; Werner, R. G.; Manosroi, W.; Manosroi, A. Transdermal Absorption and Stability Enhancement of Salmon Calcitonin by TAT Peptide. *Drug Dev. Ind. Pharm.* **2013**, *39*, 520−525.
(38) Shah, P. P.; Desai, P. R.; Channer, D.; Singh, M. Enhanced Skin Permeation Using Polyarginine Modified Nanostructured Lipid Carriers. *J. Controlled Release* **2012**, *161*, 735−745.
(39) Libster, D.; Aserin, A.; Yariv, D.; Shoham, G.; Garti, N. Concentration- and Temperature-Induced Effects of Incorporated Desmopressin on the Properties of Reverse Hexagonal Mesophase. *J. Phys. Chem. B* **2009**, *113*, 6336−6346.
(40) Sintov, A. C.; Botner, S. Transdermal Drug Delivery Using Microemulsion and Aqueous Systems: Influence of Skin Storage Conditions on the *in vitro* Permeability of Diclofenac from Aqueous Vehicle Systems. *Int. J. Pharm.* **2006**, *311*, 55−62.
(41) Cohen-Avrahami, M.; Aserin, A.; Garti, N. H-II Mesophase and Peptide Cell-Penetrating Enhancers for Improved Transdermal Delivery of Sodium Diclofenac. *Colloids Surf., B* **2010**, *77*, 131−138.
(42) Mason, P. E.; Neilson, G. W.; Dempsey, C. E.; Barnes, A. C.; Cruickshank, J. M. The Hydration Structure of Guanidinium and Thiocyanate ions: Implications for Protein Stability in Aqueous Solution. *Proc. Natl. Acad. Sci. U.S.A.* **2003**, *100*, 4557−4561.
(43) Libster, D.; Ben Ishai, P.; Aserin, A.; Shoham, G.; Garti, N. Molecular Interactions in Reverse Hexagonal Mesophase in the Presence of Cyclosporin A. *Int. J. Pharm.* **2009**, *367*, 115−126.
(44) Cohen-Avrahami, M.; Libster, D.; Aserin, A.; Garti, N. Sodium Diclofenac and Cell-Penetrating Peptides Embedded in H-II

Mesophases: Physical Characterization and Delivery. *J. Phys. Chem. B* **2011**, *115*, 10189−10197.
(45) Senatra, D.; Gabrielli, G.; Caminati, G.; Zhou, Z. Conformational-Changes at the Microemulsion Water Oil Interface and their Influence on the Systems Dielectric Temperature Behavior. *IEEE Trans. Electr. Insul.* **1988**, *23*, 579−589.
(46) Senatra, D.; Lendinara, L.; Giri, M. G. W/O Microemulsions as Model Systems for the Study of Water Confined in Microenvironments: Low-Resolution Proton Magnetic Resonance Relaxation Analysis. *Prog. Colloid Polym. Sci.* **1991**, *84*, 122−128.
(47) Senatra, D.; Lendinara, L.; Giri, M. G. Different Degrees of Hydration in Water Oil Microemulsions by Low-Resolution H-1 Magnetic-Relaxation Analysis. *Can. J. Phys.* **1990**, *68*, 1041−1048.
(48) Ezrahi, S.; Nir, I.; Aserin, A.; Kozlovich, N.; Feldman, Y.; Garti, N. Dielectric and Calorimetric Characteristics of Bound and Free Water in Surfactant-Based Systems. *J. Dispersion Sci. Technol.* **2002**, *23*, 351−378.
(49) Garti, N.; Aserin, A.; Tiunova, I.; Fanun, M. A DSC Study of Water Behavior in Water-in-Oil Microemulsions Stabilized by Sucrose Esters and Butanol. *Colloids Surf., A* **2000**, *170*, 1−18.
(50) Yaghmur, A.; Aserin, A.; Tiunova, I.; Garti, N. Sub-Zero Temperature Behaviour of Non-Ionic Microemulsions in the Presence of Propylene Glycol by DSC. *J. Therm. Anal. Calorim.* **2002**, *69*, 163−177.
(51) Zhang, J.; Yan, Y. B. Probing Conformational Changes of Proteins by Quantitative Second-Derivative Infrared Spectroscopy. *Anal. Biochem.* **2005**, *340*, 89−98.
(52) Vass, E.; Hollosi, M.; Besson, F.; Buchet, R. Vibrational Spectroscopic Detection of beta- and gamma-Turns in Synthetic and Natural Peptides and Proteins. *Chem. Rev.* **2003**, *103*, 1917−1954.
(53) Kong, J.; Yu, S. Fourier Transform Infrared Spectroscopic Analysis of Protein Secondary Structures. *Acta Biochim. Biophys. Sin.* **2007**, *39*, 549−559.
(54) Wang, Y. Q.; Boysen, R. I.; Wood, B. R.; Kansiz, M.; McNaughton, D.; Hearn, M. T. W. Determination of the Secondary Structure of Proteins in Different Environments by FTIR-ATR Spectroscopy and PLS Regression. *Biopolymers* **2008**, *89*, 895−905.
(55) Krimm, S.; Bandekar, J. Vibrational Spectroscopy and Conformation of Peptides, Polypeptides, and Proteins. *Adv. Protein Chem.* **1986**, *38*, 181−364.
(56) Shojania, S.; O'Neil, J. D. Intrinsic Disorder and Function of the HIV-1 Tat Protein. *Protein Pept. Lett.* **2010**, *17*, 999−1011.
(57) Gabizon, R.; Mor, M.; Rosenberg, M. M.; Britan, L.; Hayouka, Z.; Kotler, M.; Shalev, D. E.; Friedler, A. Using Peptides to Study the Interaction Between the p53 Tetramerization Domain and HIV-1 Tat. *Biopolymers* **2008**, *90*, 105−116.
(58) Su, Y. C.; Waring, A. J.; Ruchala, P.; Hong, M. Membrane-Bound Dynamic Structure of an Arginine-Rich Cell-Penetrating Peptide, the Protein Transduction Domain of HIV TAT, from Solid-State NMR. *Biochemistry* **2010**, *49*, 6009−6020.
(59) Li, L. B.; Vorobyov, I.; Allen, T. W. The Different Interactions of Lysine and Arginine Side Chains with Lipid Membranes. *J. Phys. Chem. B* **2013**, *117*, 11906−11920.
(60) Herce, H. D.; Garcia, A. E. Molecular Dynamics Simulations Suggest a Mechanism for Translocation of the HIV-1 TAT Peptide Across Lipid Membranes. *Proc. Natl. Acad. Sci. U.S.A.* **2007**, *104*, 20805−20810.
(61) Bitan-Cherbakovsky, L.; Libster, D.; Ottaviani, M. F.; Aserin, A.; Garti, N. Structural Behavior and Interactions of Dendrimer within Lyotropic Liquid Crystals, Monitored by EPR Spectroscopy and Rheology. *J. Phys. Chem. B* **2012**, *116*, 2420−2429.
(62) Budil, D. E.; Lee, S.; Saxena, S.; Freed, J. H. Nonlinear-Least-Squares Analysis of Slow-Motion EPR Spectra in One and Two Dimensions Using a Modified Levenberg-Marquardt Algorithm. *J. Magn. Reson., Ser. A* **1996**, *120*, 155−189.
(63) Smith, C. A.; Calabro, V.; Frankel, A. D. An RNA-Binding Chameleon. *Mol. Cell* **2000**, *6*, 1067−1076.
(64) Calnan, B. J.; Biancalana, S.; Hudson, D.; Frankel, A. D. Analysis of Arginine-Rich Peptides from the HIV TAT Protein Reveals Unusual Features of RNA Protein Recognition. *Genes Dev.* **1991**, *5*, 201−210.